On the other hand

$$\int_{z_1}^{z_N} \left|\frac{d\varphi}{dz}\right| \Big/ (\varphi^2+B^2).dz \leq (m+1)\int_{-\infty}^{+\infty} \frac{d\varphi}{\varphi^2+B^2} = \frac{\pi}{B}(m+1) \qquad \text{(B2)}$$

where m is the number of maxima and minima of $d\varphi/dz$ between z_N and z_1. Thus, it follows that

$$|I_{11}^{(2n)}| \leq \frac{1}{(2n)!}\{(m+1)\tfrac{1}{2}\pi\}^{2n}. \qquad \text{(B3)}$$

In a similar way

$$|I_{11}^{(2n+1)}| \leq \frac{1}{(2n+1)!}\{(m+1)\tfrac{1}{2}\pi\}^{2n+1}. \qquad \text{(B4)}$$

Therefore we can see $\Sigma I_{ij}^{(2n)}$ and $\Sigma I_{ij}^{(2n+1)}$ converge absolutely.

The author would like to express his sincere thanks to Dr A. R. Lang for his valuable discussion and kind encouragement throughout this work. He also wishes to express his thanks to Dr J. W. Menter, Dr P. B. Hirsch, Dr M. J. Whelan and Dr A. Howie who kindly gave him opportunities of seeing their interesting electron micrographs.

References

BORRMANN, G., HARTWIG, W. & IRMLER, H. (1958). *Z. Naturforsch.* **139**, 423.
EWALD, P. P. (1958). *Acta Cryst.* **11**, 888.
HASHIMOTO, H. & MANNAMI, M. (1960). *Acta Cryst.* **13**. 363.
HASHIMOTO, H. HOWIE, A. & WHELAN, J. M. (1960). *Phil. Mag.* **5**, 967.
HEIDENREICH, R. D. (1949). *J. Appl. Phys.* **20**, 993.
HILDEBRANDT, G. (1959). *Z. Kristallogr.* **112**, 312.
HIRSCH, P. B., HORNE, R. W. & WHELAN, M. J. (1956). *Phil. Mag.* **1**, 677.
HIRSCH, P. B., HOWIE, A. & WHELAN, M. J. (1960). *Phil. Trans. Roy. Soc. Lond.* **252**, 499.
HOWIE, A. & WHELAN, M. J. (1961). *Proc. Roy. Soc.* A, **263**, 217.
HUNTER, L. P. (1959). *J. Appl. Phys.* **30**, 874.
ISHII, Z. & KOHRA, K. (1959). *J. Phys. Soc. Japan*, **14**, 1250.
KAMIYA, Y. & UYEDA, R. (1961). *J. Phys. Soc. Japan.* **16**, 1361.
KATO, N. (1952). *J. Phys. Soc. Japan*, **7**, 397.
KATO, N. (1958). *Acta Cryst.* **11**, 885.
KATO, N. (1961*a*). *Acta Cryst.* **14**, 526.
KATO, N. (1961*b*). *Acta Cryst.* **14**, 627.
KATO, N. (1963). *Acta Cryst.* **16**, 276.
KOEHLER, J. S. (1941). *Phys. Rev.* **60**, 397.
LANG, A. R. (1958). *J. Appl. Phys.* **29**, 597.
LANG, A. R. (1959*a*). *J. Appl. Phys.* **30**, 1748.
LANG, A. R. (1959*b*). Private communication.
LAUE, M. v. (1952). *Acta Cryst.* **5**, 619.
LAUE, M. v. (1953). *Acta Cryst.* **6**, 217.
MENTER, J. W. (1960). Private communication.
NEWKIRK, J. B. (1958). *Phys. Rev.* **110**, 1465.
WARREN, B. E. & AVERBACH, B. L. (1950). *J. Appl. Phys.* **21**, 595.
WILSON. A. J. C. (1952). *Acta Cryst.* **5**, 318.

Acta Cryst. (1963). **16**, 290

Electron Diffraction Study on Thin Films of Polymers of *p*-Halogeno-styrene

BY KINYA KATADA*

Faculty of Science, Osaka City University, 12 *Minami-ogimachi, Kita-ku, Osaka, Japan*

(*Received* 23 *October* 1961 *and in revised form* 7 *March* 1962)

Thin films of polymers of *p*-Cl-, *p*-Br- and *p*-I-styrene obtained by radical polymerization were studied by electron diffraction. Ten to thirteen halos were obtained by using a sector-camera. Intensity curves for some assumed models were calculated and were compared with the observed ones. In the cases of the Br- and I-derivatives the complex atomic scattering factors were used for the calculation. The radial distribution method was applied to the Cl-derivative.

The following results are common to all three kinds of halogen derivatives. A linear molecule is built up of styrene residues connected in a 'head to tail' arrangement, and their benzene rings are located alternately on each side of the plane of the zig-zag paraffin chain. Neighboring molecules are closely packed in a 'face to face' configuration in a plane perpendicular to the chain. These regularities in the structure are maintained only among the nearest neighbor residues.

1. Introduction

Several electron diffraction studies of amorphous thin films have been reported. Since more halos can be obtained by electron diffraction than by X-ray diffraction, the former method is better suited to a structure analysis of the shorter interatomic distances. There have been few studies, however, in which this usefulness of electron diffraction has been exploited. In the present study, this merit of electron diffraction

* Present address: Faculty of Science, Osaka City University, Sugimotocho, Sumiyoshi-ku. Osaka, Japan.

will be used and a practical method of analysis will be described.

In a study on thin films of polystyrene, agar, gelatin, methyl-, acetyl-, nitro- and benzyl-cellulose, Kakinoki, Murata & Katada (1949) found similar electron diffraction patterns with six to eight halos for each substance.* This similarity was explained by considering that the constituent atoms in these 'light' substances arranged with similar interatomic distances and scattering powers within each compound even though their overall chemical structures differed greatly. Kakinoki (1949) analyzed the halo pattern from thin films of polystyrene in detail and determined the relative position of benzene rings along the chain of polystyrene, but he was not able to get any conclusion about the intermolecular configuration. The latter information may be derived, however, if light atoms at certain positions in a polystyrene molecule are substituted by heavy atoms. For this reason polymers of *p*-halogen derivatives of styrene (polymers of *p*-Cl-, *p*-Br- and *p*-I-styrene) have been studied by electron diffraction.

2. Experimental

The samples were synthesized by a method of radical polymerization.† Thin films were prepared by allowing a drop of dilute benzene solution of polymer to evaporate from a clean water surface. They were then transferred onto a brass specimen holder with several holes of 0·5 mm diameter. The films were estimated to be of the order of hundreds of Ångströms in thickness.

An electron diffraction camera with a rotating sector (Ino, 1953) was operated under accelerating voltages between 40 and 60 kV.

The films of halogen derivatives were weaker than those of polystyrene. The use of a surface of warm water was somewhat helpful for making a film stronger and more uniform, but in the cases of the Br- and I-derivatives it was very difficult to prepare a film thin enough to produce a diffraction pattern with high contrast. In spite of this situation more than ten halos were visually observed on the photographs taken with the sector-camera. A quantitative intensity measurement of the diffraction pattern by the usual microphotometric technique was only available for the Cl-derivative.

The densities of these films were assumed to be the same as those of small bulk samples which were measured by the floating method. They were 1·20, 1·56 and 1·87 g.cm.$^{-3}$ for the Cl-, Br- and I-derivatives, respectively.‡

* It was found by Ino that some proteins such as egg-albumin, silk-fibroin and casein showed similar results (unpublished).

† The author is indebted to Prof. A. Kotera of Tokyo University of Education for the supply of the samples.

‡ The density of polystyrene is 1·05 g.cm.$^{-3}$.

3. Intensity data

For the Cl-derivative the structure sensitive intensity, $I(s)$, was obtained from the observed total intensity as follows:

$$I(s)=C\{[\text{total intensity/background intensity}]-1\}, \quad (1)$$

where C is a constant, which will be given in Sec. 4, and $s=(4\pi/\lambda)\sin(\theta/2)$, λ being the wave-length of the primary electron beams and θ the scattering angle.

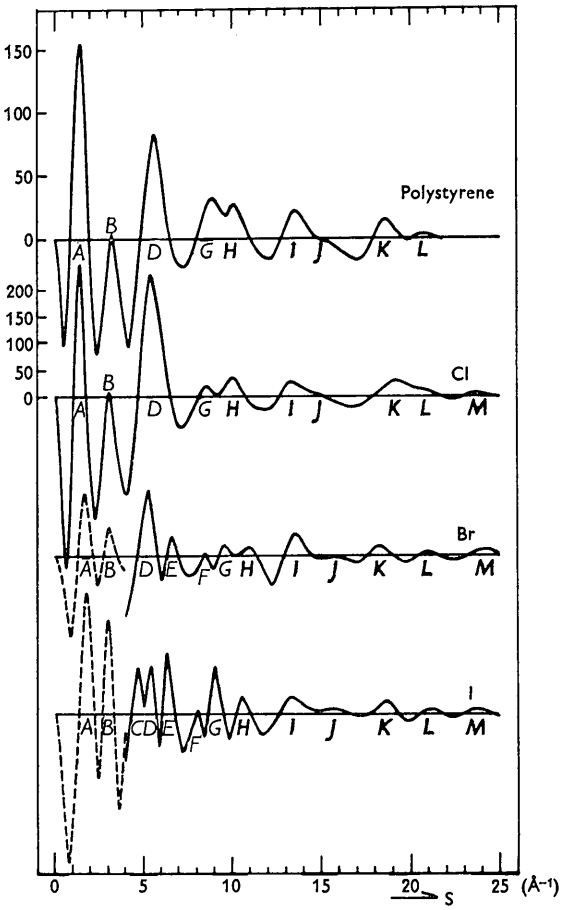

Fig. 1. Experimental intensity curves, $I(s)$, for polystyrene and its *p*-Cl-derivative obtained with the sector-microphotometric procedure and for the *p*-Br- and *p*-I-derivatives obtained with the sector-visual procedure. The ordinates of the parts shown with broken lines are multiplied by about a quarter.

The background intensity was determined by successive approximations, after which a reasonable radial distribution curve was obtained (sector-microphotometric procedure) (Karle & Karle, 1949, 1950). For the Br- and I-derivatives the structure sensitive intensity, $I(s)$, was estimated visually (sector-visual procedure). These intensity curves are illustrated in Fig. 1, and the s-values of the intensity maxima are listed in Table 1. For comparison, the result for

Table 1. *The s-values of maxima on the experimental intensity curves, $I(s)$, of polystyrene, its p-Cl-, p-Br- and p-I-derivatives*

σ is the standard deviation of the visually measured values of the maxima

Symbol of maximum	Polystyrene s-Value	Cl-derivative s-Value	Br-derivative s-Value	Br-derivative σ	I-derivative s-Value	I-derivative σ
A	1·38 Å^{-1}	1·43 Å^{-1}	1·71 Å^{-1}	0·011 Å^{-1}	1·81 Å^{-1}	0·008 Å^{-1}
B	3·05	3·05	3·02	0·013	2·98	0·017
C					4·70	0·012
D	5·59	5·34	5·23	0·022	5·39	0·015
E			6·48	0·014	6·32	0·026
F			8·40	0·024	8·05	0·041
G	8·80	8·55	9·45	0·034	9·04	0·044
H	10·03	10·10	10·95	0·027	10·51	0·060
I	13·48	13·29	13·64	0·030	13·35	0·072
J	15·4	15·0	15·9		15·4	
K	18·38	18·95	18·20	0·065	18·66	0·102
L	20·42	20·8	20·99	0·070	21·1	
M		23·80	24·41	0·050	23·7	

polystyrene obtained with the sector-microphotometric procedure by Ino (1953) is also shown. In the visual procedure the s-values of the maxima were determined by averaging over values measured on several photographic plates for each derivative. The standard deviations of these values are also listed in Table 1.

As seen from Fig. 1, the pattern obtained from the Cl-derivative resembles over the whole region of s the pattern from polystyrene, which has intensity features common to the 'light' substances mentioned in Sec. 1. But the Br- and I-derivatives produce patterns different from that of polystyrene, especially in the region of $4<s<12$ Å^{-1}. The additional maxima E and F appear in the case of the Br-derivative and C, E and F in the case of the I-derivative.

4. Calculation of the intensity curves

Intensity formula

Except in the region of very small values of s, the total intensity, $J_t(s)$, of electrons diffracted by amorphous material is expressed as follows:

$$\begin{aligned} J_t(s) &= NB(s)\{I_a(s)+I_i(s)+I_m(s)\} \\ &= NB(s)\left\{\sum_A n_A(Z_A-f_A(s))^2+\sum_A n_A S_A(s) \right. \\ &\quad +\frac{N}{V}\sum_A\sum_B n_A n_B(Z_A-f_A(s))(Z_B-f_B(s)) \\ &\quad \left.\times\int_0^\infty 4\pi r^2(W_{AB}(r)-1)\frac{\sin sr}{sr}\,dr\right\}, \end{aligned} \tag{2}$$

where $B(s)=(J_0/R^2)(8\pi^2me^2/h^2)^2(1/s^4)$, each symbol having its usual meaning. V is the effective volume of specimen for scattering of electrons, N the number of certain units of the chemical constitution (repeating units) in the volume V, n_A the number of atoms of the A-type in a repeating unit, Z_A the atomic number, $f_A(s)$ the atomic scattering factor for X-rays, and $S_A(s)$ the incoherent intensity function for X-rays for an atom of the A-type, $4\pi r^2W_{AB}(r)dr/V$ a probability function that an atom of the B-type is at a distance between r and $r+dr$ from an atom of the A-type and $\sum_A$ means the summation over the types of atoms. The sum of the first two terms in equation (2) represents the background intensity.

If Z_A is substituted for $(Z_A-f_A(s))$, $I_m(s)$ in equation (2) becomes the reduced structure sensitive intensity per repeating unit, $I(s)$, namely,

$$\begin{aligned} I(s) &= (N/V)\sum_A\sum_B n_A n_B Z_A Z_B \\ &\quad \times\int_0^\infty 4\pi r^2(W_{AB}(r)-1)(\sin sr/sr)\,dr\,. \end{aligned} \tag{3}$$

Each atom within a repeating unit is labelled by a different subscript, and this labelling is retained in each repeating unit. Since $W_{AB}(r)$ tends to unity beyond a certain value of r, say l_{AB}, the following expression can be obtained for $I(s)$:

$$\begin{aligned} I(s) &= \sum_i^{\text{unit}}\sum_j^{\prime\, r_{ij}<l_{AB}} Z_i Z_j \exp(-\Delta_{ij}s^2)\frac{\sin sr_{ij}}{sr_{ij}} \\ &\quad -(N/V)\sum_{(AB)}(2-\delta_{AB})n_A n_B Z_A Z_B \\ &\quad \times\int_0^{l_{AB}} 4\pi r^2\frac{\sin sr}{sr}\,dr, \end{aligned} \tag{4}$$

where r_{ij} is the interatomic distance between the ith and jth atoms, $\exp(-\Delta_{ij}s^2)$ the damping factor due to thermal vibrations or to fluctuation in the distance r_{ij}, $\delta_{AB}=0$ for $A\neq B$, $\delta_{AB}=1$ for $A=B$, $\sum_i^{\text{unit}}$ means the summation over all atoms in a repeating unit, $\sum_j^{\prime\, r_{ij}<l_{AB}}$ the summation over all atoms for which $0<r_{ij}<l_{AB}$, regardless whether the jth atom is in or not in the repeating unit containing the ith atom, and $\sum_{(AB)}$ the summation over the types of atomic pairs.

If the constant C in equation (1) is defined as

$$C=\sum_A\{n_A Z_A^2+n_A Z_A\}, \tag{5}$$

equation (1), the experimental intensity, becomes equal to equations (3) or (4) under the assumption that

$$Z_A - f_A(s) = Z_A\varphi(s),\ S_A(s) = Z_A\varphi^2(s)\ , \qquad (6)$$

where $\varphi(s)$ is a certain function of s common to all types of atoms. This approximation is permissible except in the region of small s. The experimental intensity obtained by the sector-visual procedure can also be compared with the intensity calculated from equation (4) because of the nature of the human eye (Pauling & Brockway, 1934).

Models and calculation procedure

Kakinoki (1949) considered four models for polystyrene which are illustrated in Fig. 2. He determined model I to be the best, and therefore it is the only model used to calculate the summation term in equation (4) for the halogen derivatives.

In model I many styrene residues form a 'head to tail' connection and their benzene rings are located alternately on each side of the plane of the zig-zag paraffin chain. Two styrene residues, $C_{16}H_{14}X_2$, were taken as a repeating unit, where X is a halogen atom. Normal values for bond distances and bond angles were assumed, for example, 1·09 Å for C–H distance,

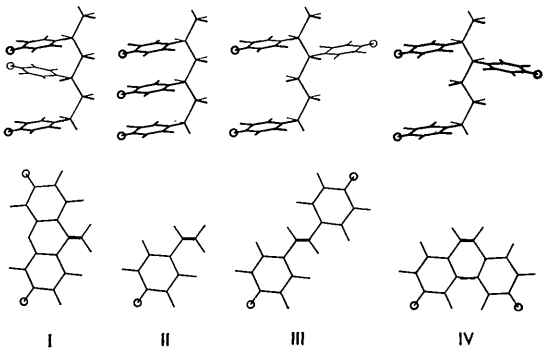

Fig. 2. Schematic side views (upper) and plans (lower) of the four models considered for polystyrene. Circles show the positions of H-atoms where halogen atoms are substituted. Thick line in the plan shows the projection of paraffin chain.

Table 2. *The values of the C–X distances (a) and of the X–X distances (b) in the models considered*

(*a*)

	C–Cl	C–Br	C–I
Model I′	1·76 Å	1·91 Å	2·10 Å
Model I″	1·69	1·85	2·05

(*b*)

	Cl–Cl			Br–Br			I–I		
	(i)	(ii)	(iii)	(i)	(ii)	(iii)	(i)	(ii)	(iii)
Model I_a	4·40 Å	4·50 Å	5·04 Å	4·55 Å	4·65 Å	5·04 Å	4·58 Å	4·68 Å	5·04 Å
Model I_b	3·60	5·16	5·04	3·90	5·11	5·04	4·30	4·77	5·04
Model I_c	3·60	4·84	5·04	3·90	4·85	5·04	4·30	4·93	5·04

Table 3. *The values of* l_{AB}, Z_AZ_B, $\Psi = \sum_{(AB)} \psi_{AB}$, $\Psi^* = \sum_{(AB)} \psi^*_{AB}$ *and* $\Delta\Psi = \Psi^* - \Psi = \sum_{(AB)} \Delta\psi_{AB}$ *for the* Cl-, Br- *and* I-*derivatives*

Values of $n_{AB} = \psi_{AB}/Z_AZ_B$, $n_{AB}{}^* = \psi_{AB}{}^*/Z_AZ_B$ and $\Delta n_{AB} = \Delta\psi_{AB}/Z_AZ_B$ in parentheses are twice as large as the number of distances which belong to each group. (An interatomic distance between different repeating units is counted as a half)

A–B	l_{AB}	Z_AZ_B	ψ_{AB}	(n_{AB})	$\psi_{AB}{}^*$	$(n_{AB}{}^*)$	$\Delta\psi_{AB}$	(Δn_{AB})
				Cl-derivative				
C–C	4·00 Å	36	6048	(168)	6577	(182·7)	529	(14·7)
C–H	3·20	6	1080	(180)	964	(160·7)	−116	(−19·3)
C–Cl	3·80	102	1224	(12)	3919	(38·4)	2695	(26.4)
H–Cl	3·00	17	136	(8)	281	(16·5)	145	(8·5)
Cl–Cl	6·00	289	3468	(12)	2731	(9·4)	−737	(−2·6)
			$\Psi = 11956$,		$\Psi^* = 14472$,		$\Delta\Psi = 2516$	
				Br-derivative				
C–C	4·00 Å	36	6048	(168)	6345	(176·4)	297	(8·4)
C–H	3·20	6	1080	(180)	948	(158·1)	−132	(−21.9)
C–Br	3·95	210	2520	(12)	8910	(42.4)	6390	(30.4)
H–Br	3·15	35	280	(8)	660	(18·9)	380	(10·9)
Br–Br	6·00	1225	14700	(12)	11390	(9·3)	−3310	(−2·7)
			$\Psi = 24628$,		$\Psi^* = 28253$,		$\Delta\Psi = 3625$	
				I-derivative				
C–C	4·00 Å	36	6048	(168)	6051	(168·1)	3	(0·1)
C–H	3·20	6	1080	(180)	905	(150·8)	−175	(−29·3)
C–I	4·15	318	3816	(12)	14940	(47·0)	11124	(35·0)
H–I	3·35	53	424	(8)	1145	(21·6)	721	(13·6)
I–I	6·00	2809	33708	(12)	24900	(8·9)	−8808	(−3·1)
			$\Psi = 45076$,		$\Psi^* = 47941$,		$\Delta\Psi = 2865$	

1·39 Å for aromatic C–C, 1·54 Å for aliphatic C–C, 120° for aromatic carbon angle and 109·5° for aliphatic. Two values were, however, assumed for C–X bond distance. In model I′ the C–X bond distance was set equal to the sum of the covalent bond radii of carbon and halogen atoms (Pauling, 1960) and in model I″ it was given the value found in halogen derivatives of benzene (Sutton, 1958). These values are listed in Table 2(*a*). The value of l_{AB}, except for the X–X pair, was assumed to be equal to the van der Waals distance of the A–B pair, as listed in Table 3 (Pauling, 1960). The value of l_{XX} will be given below.

The plan of two successive residues of model I with atoms shown as van der Waals spheres yields an area of 78·8 Å^2 for the Cl-derivative. But the average area calculated from the value of the density is 76·1 Å^2 per repeating unit, showing that the molecules may be closely packed. Similar results are obtained for polystyrene and its other two halogen derivatives. Three models, I_a, I_b and I_c, for the lateral arrangement of molecules were considered for each derivative as shown in Fig. 3, where the neighboring molecules were packed until the van der Waals spheres of the

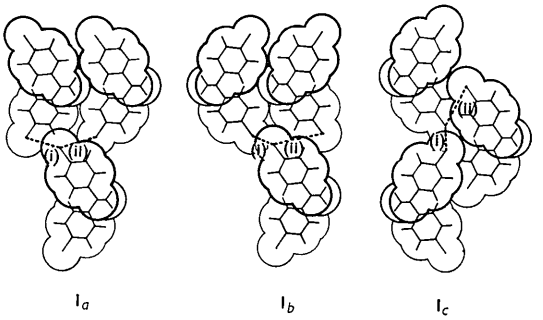

Fig. 3. Three models for the relative configuration of neighboring molecules for model I of the Cl-derivative. Thick, medium (–CH_2–) and thin curves show the sections of van der Waals spheres cut by three successive planes perpendicular to the chain with intervals of 1·26 Å. Broken lines show two of the three kinds of Cl–Cl distances taken into the calculation of intensity.

outer atoms came in contact with each other. Several distances for the X–X pair were calculated from these models, and the value of l_{XX} was assumed to be 6·0 Å for all derivatives. The X–X distances actually taken into the summation term are tabulated in Table 2(*b*), where (i) and (ii) are the distances shown in Fig. 3 and (iii) is the distance between the two halogen atoms in a molecule which lie one above the other in the direction parallel to the chain.

Thus, the summation term in equation (4) is conveniently separated into two terms, $I_1(s)$ and $I_2(s)$, where $I_1(s)$ is the sum of the contributions from all distances shorter than l_{AB} except X–X distances and $I_2(s)$ the contribution from X–X distances shorter than l_{XX}.

The values of N/V estimated from the observed values of the densities are $2{\cdot}61\times10^{-3}$, $2{\cdot}57\times10^{-3}$ and $2{\cdot}45\times10^{-3}$ Å^{-3} for Cl-, Br- and I-derivatives, respectively. The integral in equation (4) is transformed to $(4\pi/3)l_{AB}^3\Phi(sl_{AB})$ where $\Phi(x)=3\,(\sin x - x\cos x)/x^3$. Thus, the integral term, $I_3(s)$, can be easily evaluated.

There is another point to be considered here. The total scattering power, Ψ, which is the sum of Z_AZ_B for atomic pairs included in the summation term is given in Table 3 along with its component ψ_{AB}. As seen from Table 3, ψ_{AB} deviates in general from

$$\psi^*_{AB}=(2-\delta_{AB})(N/V)n_An_BZ_AZ_B\int_0^{l_{AB}}4\pi r^2dr$$
$$=(2-\delta_{AB})(N/V)n_An_BZ_AZ_B\cdot\tfrac{3}{4}\pi l_{AB}^3\,, \qquad (7)$$

and therefore the difference $\Delta\psi_{AB}=\psi^*_{AB}-\psi_{AB}$ should

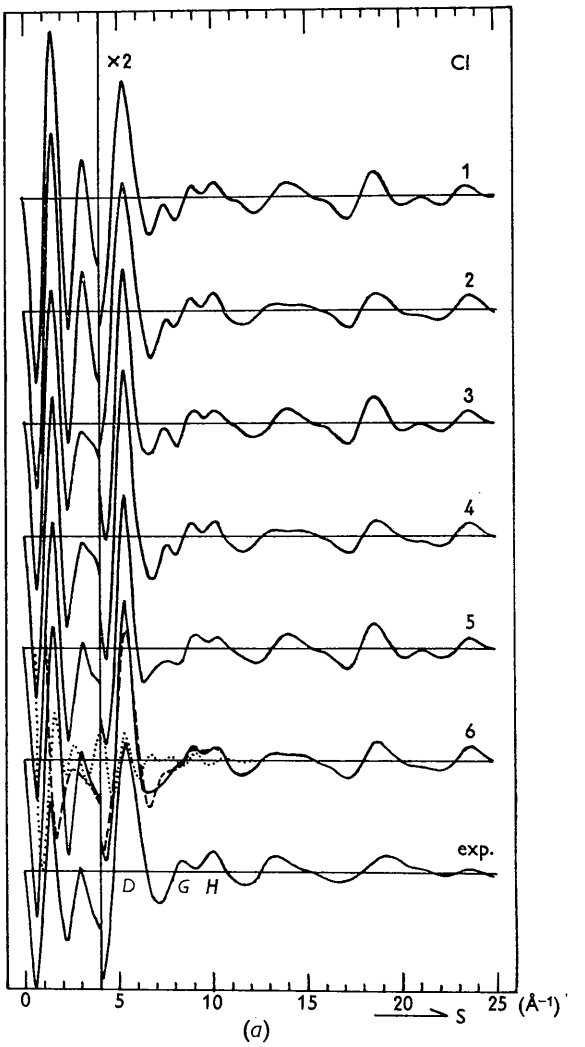

Fig. 4. Comparison between the calculated and the experimental intensities for the Cl-derivative (*a*), the Br-derivative (*b*) and the I-derivative (*c*). The calculated curves 1, 2, 3, 4, 5 and 6 correspond to the models I_a', I_a'', I_b', I_b'', I_c' and I_c'', respectively. Broken and dotted lines in curves 6 show the summation terms $I_1(s)$ and $I_2(s)$, respectively. The ordinates beyond $s=4$ Å^{-1} are multiplied by two, four and ten for (*a*), (*b*) and (*c*), respectively.

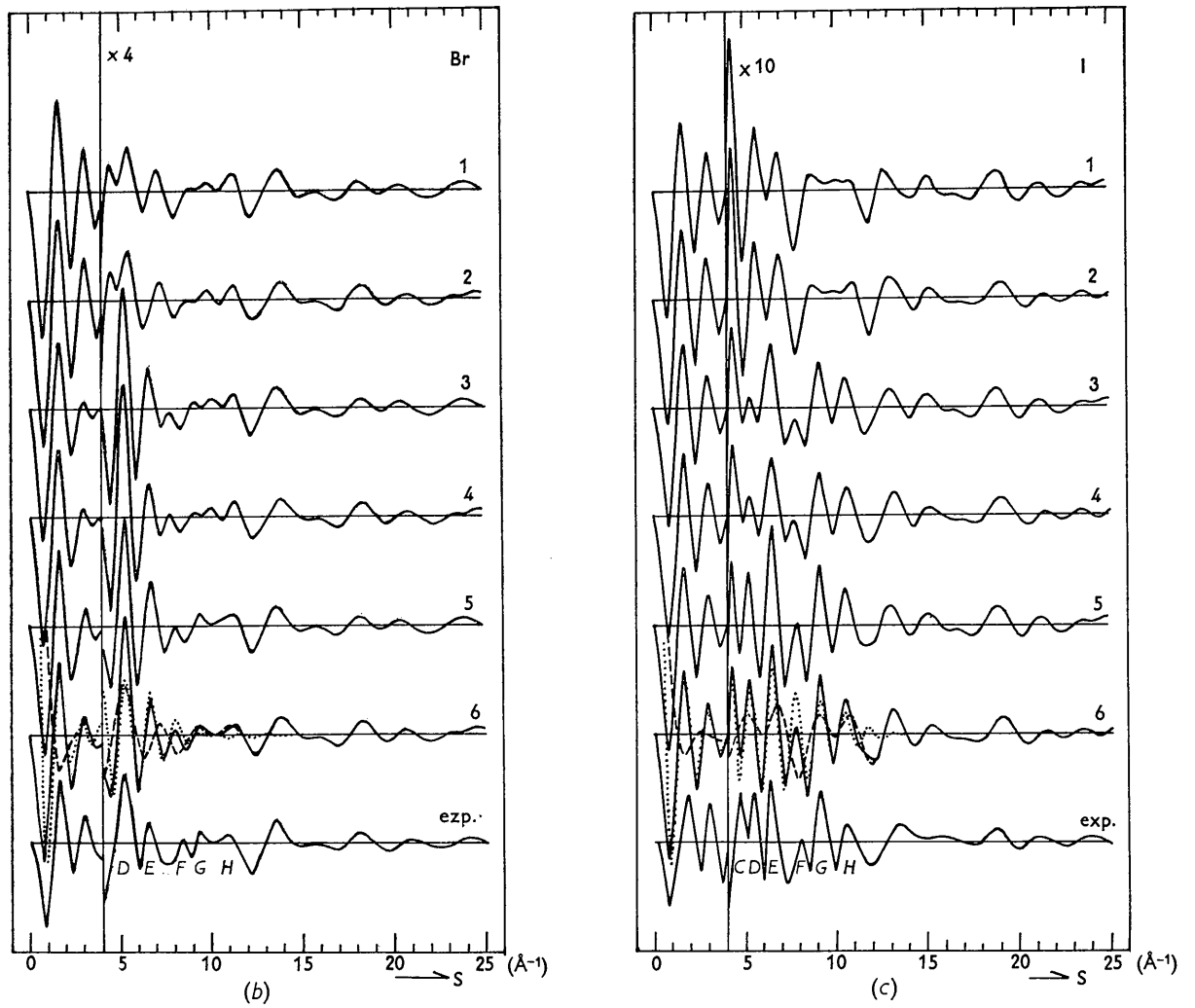

Fig. 4 (cont.)

be appropriately taken into consideration. These values are also listed in Table 3. The residual scattering power, $\Delta\Psi = \Psi^* - \Psi = \sum_{(AB)} \Delta\psi_{AB}$, was simply assigned to a few distances larger than l_{AB} as follows:

Cl-derivative

$r_1 = 3{\cdot}80$ Å	$\Delta\Psi_1 = 1000$
$r_2 = 4{\cdot}00$	$\Delta\Psi_2 = 600$
$r_3 = 4{\cdot}50$	$\Delta\Psi_3 = 300$
$r_4 = 4{\cdot}00$	$\Delta\Psi_4 = 300$
$r_5 = 5{\cdot}04$	$\Delta\Psi_5 = 300$

Br-derivative		I-derivative	
$r_1 = 3{\cdot}95$ Å	$\Delta\Psi_1 = 1800$	$r_1 = 4{\cdot}15$ Å	$\Delta\Psi_1 = 1500$
$r_2 = 4{\cdot}15$	$\Delta\Psi_2 = 1200$	$r_2 = 4{\cdot}33$	$\Delta\Psi_2 = 900$
$r_3 = 4{\cdot}67$	$\Delta\Psi_3 = 600$	$r_3 = 4{\cdot}85$	$\Delta\Psi_3 = 450$

where $r_1 = l_{CX}$, r_2 and r_3 are the C–X distances separated by two and three carbon atoms in a benzene ring, respectively, $r_4 = l_{CC}$ and r_5 is the C–C distance between two benzene rings.* The correction term

$$\Delta I(s) = \sum_n \Delta\Psi_n \sin sr_n / sr_n \qquad (8)$$

was added to equation (4).

Mean deviations, $(2\Delta_{ij})^{\frac{1}{2}}$, were assumed to be 0·05 Å for the bond distances, 0·08 Å for the distances separated by one atom, 0·12 Å for those separated by two or more atoms and 0·23 Å for those used in $I_2(s)$ and $\Delta I(s)$. But in the actual calculation the bond distances were not multiplied by the damping factor, and the relative values of 0·03, 0·07 and 0·18 Å were used as the mean deviations for the other groups of the distances, respectively.

The contribution of H–H pairs to the intensity was entirely neglected.

* The values of r_2 and r_3 used here are the averages of the corresponding values in models I′ and I″.

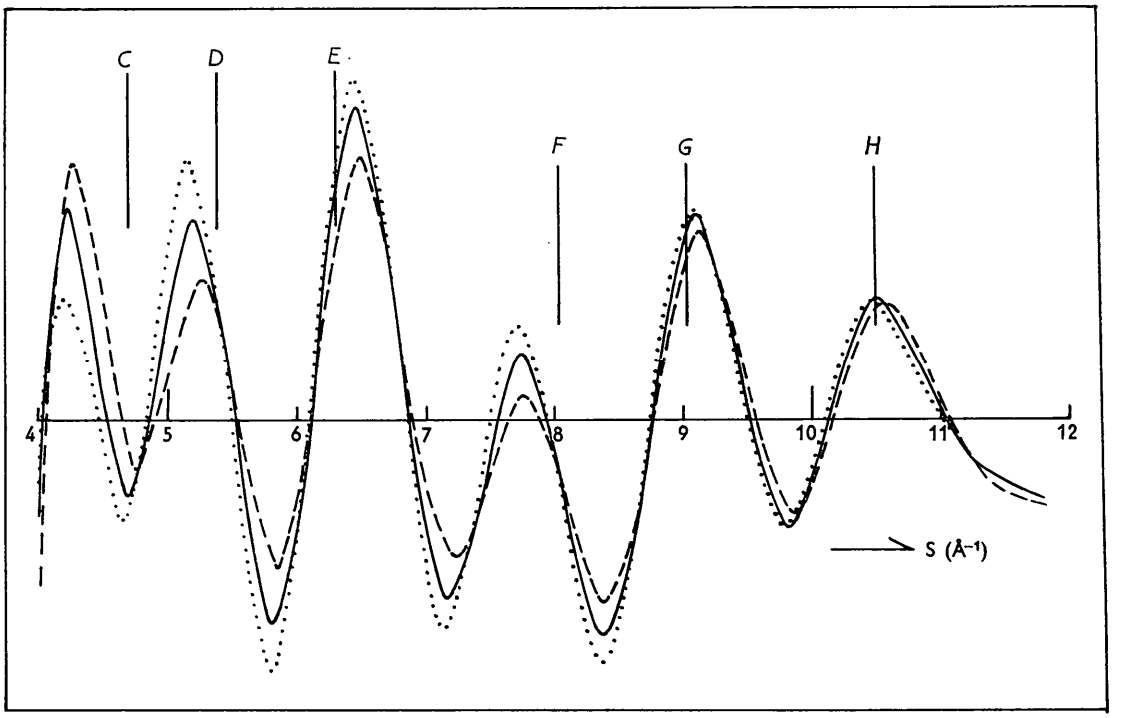

Fig. 5. Calculated intensity curves for the I-derivative with the three sets of I–I distances (i), (ii) and (iii) of 4·33, 4·85 and 5·04 Å (broken line), 4·33, 4·93 and 5·04 Å (full line) and 4·36, 5·00 and 5·04 Å (dotted line). Vertical lines show the positions of the observed intensity maxima.

Comparison between the observed and the calculated intensities

The intensities, $I_1(s)+I_2(s)-I_3(s)+\Delta I(s)$, calculated above were compared with the experimental one. Fig. 4 shows the comparison for Cl-, Br- and I-derivatives. It can be concluded that model I_c'' is the best for all of the halogen derivatives.

Model I_a for Br- and I-derivatives gives intensity curves which clearly do not coincide with the observed ones in the region of $4<s<12$ Å^{-1}. Model I_b for the Br-derivative also fails to reproduce the observed intensity features in that region. But model I_b for the I-derivative reproduces the observed features as well as model I_c does except for the intensity ratio between maxima *C* and *D*. Hence models I_a and I_b are not acceptable, but the selection between models I_c' and I_c'' is difficult in these cases, the latter being somewhat more probable. In the case of the Cl-derivative the difference between the intensities given by the intramolecular models I′ and I″ is larger than that among the intensities given by the intermolecular models I_a, I_b and I_c. It can be easily seen from Fig. 4 that model I_c'' is the best for the Cl-derivative, too.

Some attempts were made to determine the spacing between neighboring molecules. For the I-derivative the I–I distances considered were

(i)	(ii)	(iii)	
4·30 Å	4·70 Å	5·04 Å	
4·30	4·77	5·04	(model I_b)
4·33	4·85	5·04	
4·33	4·93	5·04	(model I_c)
4·36	5·00	5·04	
4·36	5·07	5·04	

Fig. 5 shows three of the intensity curves calculated from these sets. The fourth set corresponding to model I_c gives the best intensity ratio between maxima *C* and *D*, but the slight disagreement in the positions of these maxima between the observed and the calculated intensities could not be improved by the use of the above sets of distances.

The values of the mean deviations were changed also, and the relative value of 0·18 Å was found to be better than that of 0·15 or 0·20 Å for $I_2(s)$ and $\Delta I(s)$.

The contributions from each term of the intensity calculated with the best model I_c'' are summarized here.* For all of the halogen derivatives, $I_1(s)$, the intensity due to distances within a repeating unit, reproduces well the observed intensity features for $s>13$ Å^{-1} as seen in Fig. 4. The contribution from $I_2(s)$ is dominant for $s<12$ Å^{-1} for the heavy halogen

* Kakinoki (1949) explained successfully the observed intensity features of polystyrene by the contributions from the four component groups of $I_1(s)$. The numbers and the positions of maxima and minima, except for the first maximum, were mainly given by the contributions from the next nearest neighbor distances, and their relative intensities mainly by the nearest neighbor distances. In his paper, however, nothing was described about the subgroups of $I_1(s)$.

derivatives and is negligibly small outside this region. The contribution from $I_1(s)$ to maximum D decreases with the increase in the atomic number of the halogen atom, and in the case of the I-derivative it is overcome by the contribution from $I_2(s)$, forming a doublet, C and D. The weakness of the observed maximum F is due to a deep minimum in $I_1(s)$. Although maxima G and H lie at different positions for the different derivatives and polystyrene, they are constituted by the contributions from $I_1(s)$ and $I_2(s)$ in a similar way for all derivatives.

The integral term, $I_3(s)$, and the correction term, $\Delta I(s)$, are not shown in Fig. 4 in order to avoid confusion. $I_3(s)$, which does not exist in the case of gaseous molecules, is responsible for the appearance of the distinct first maximum A and the deep minimum inside it, but it does not contribute appreciably to the region of larger s. $\Delta I(s)$ is important only for refinement of the intensity features.

Complex atomic scattering factor for electrons

As was suggested by Glauber & Schomaker (1953), it is necessary to use the complex atomic scattering factor, $F(\theta)=|F(\theta)|\exp(i\eta(\theta))$, instead of the real one when the substance contains both light and heavy atoms. Thus, the contribution of an atomic pair i–j to the intensity is proportional to

$$2|F_i(\theta)||F_j(\theta)|\exp(-\Delta_{ij}s^2)\times\cos(\eta_i(\theta)-\eta_j(\theta))\sin sr_{ij}/sr_{ij}\,. \quad (9)$$

The calculation of the intensity was carried out using Z_i instead of $|F_i(\theta)|$ in the above formula. The numerical values of $\eta_i(\theta)$ for the present accelerating voltage of 59 kV were calculated from the table given by Ibers & Hoerni (1954). The results for the I-derivative are shown in Fig. 6, where only $I_1(s)$ is plotted for $s>12$ Å^{-1} because of the large effect of $\cos(\eta_i(\theta)-\eta_j(\theta))$ and of the negligible contribution from other terms in that region. The agreement of the positions of maxima on the calculated intensity curve with those on the observed one is much better with the complex scattering factors than with the real ones. It is more evident in Fig. 6 than in Fig. 4(*c*) that model I″ is more probable than model I′. A similar improvement was also obtained for the Br-derivative.

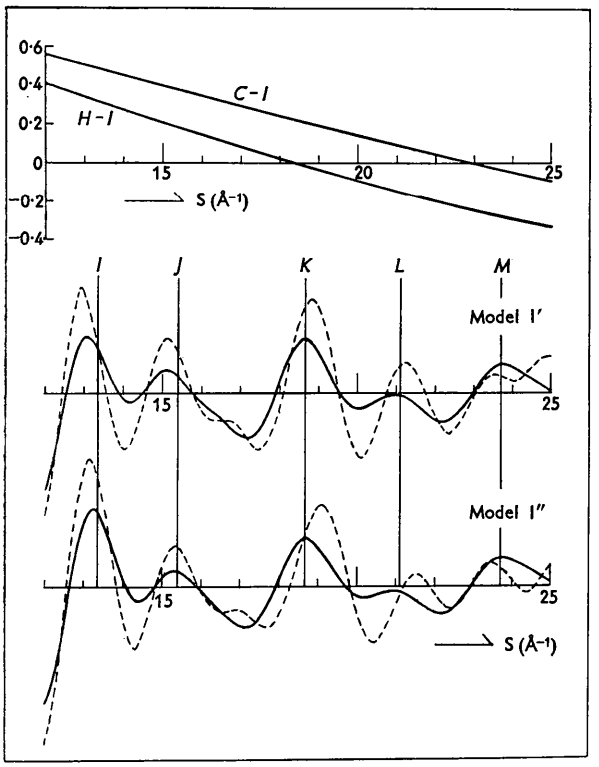

Fig. 6. Curves of $\cos(\eta_i(\theta)-\eta_j(\theta))$ for C–I and H–I pairs (upper) and calculated intensities with the complex atomic scattering factor for models I′ and I″ of the I-derivative (lower, full curves). Broken curves show those with the real atomic scattering factor (Fig. 4(*c*)), and vertical lines show the positions of the observed intensity maxima.

5. Radial distribution analysis

The radial distribution analysis was carried out only for the Cl-derivative for which the intensity was measured quantitatively.

The Fourier inversion of the structure sensitive intensity equation (3) or equation (4) gives the proper nuclear radial distribution function as follows:

$$\begin{aligned}4\pi rD^z(r)-4\pi rD_0^z&=(2/\pi)\int_0^\infty sI(s)\exp(-as^2)\sin srds\\&=\sum_i^{\text{unit}}\sum_j^{\infty\,\prime}\frac{Z_iZ_j}{r_{ij}}\{4\pi(a+\Delta_{ij})\}^{-\frac{1}{2}}\\&\quad\times\exp\{-(r-r_{ij})^2/4(a+\Delta_{ij})\}-4\pi r\left(\frac{N}{V}\right)\left(\sum_A n_AZ_A\right)^2,\end{aligned} \quad (10)$$

where the 1st and the 2nd terms come from the 1st and the 2nd ones in equation (4), respectively, and the factor $\exp(-as^2)$ is multiplied as usual in order to diminish the termination effect. Due to the failure of the approximation of equation (6) (Katada, 1958), the Fourier inversion of the experimental intensity $I_{\text{exp}}(s)$, equation (1), gives a distribution function other than the proper one. The distribution $4\pi r\Delta(r)$ should be interpreted as

$$\begin{aligned}4\pi r\Delta(r)&=4\pi rD(r)-4\pi rD_0\,,\\&=\tfrac{1}{2}\pi\int_0^\infty sI_{\text{exp}}(s)\exp(-as^2)\sin srds\\&=4\pi rD^z(r)+\sum_{k=1}\sum_i^{\text{unit}}\sum_j^{\infty\,\prime}A_{ij,k}(Z_iZ_j/r_{ij})\\&\quad\times\{4\pi(a_{ij,k}+\Delta_{ij})\}^{-\frac{1}{2}}\\&\quad\times\exp\{-(r-r_{ij})^2/4(a_{ij,k}+\Delta_{ij})\}\\&\quad-4\pi rD_0^z-4\pi r(N/V)\sum_i^{\text{unit}}\sum_j Z_iZ_j\sum_{k=1}A_{ij,k}\end{aligned} \quad (11)$$

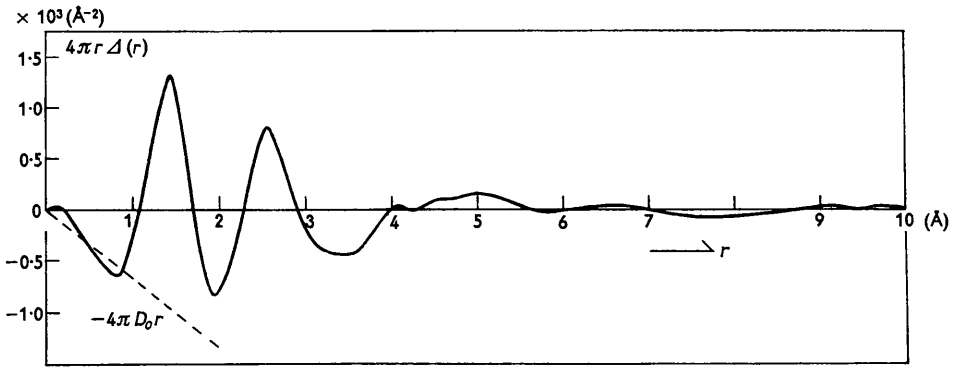

Fig. 7. Curve of $4\pi r\Delta(r)$ for the Cl-derivative.

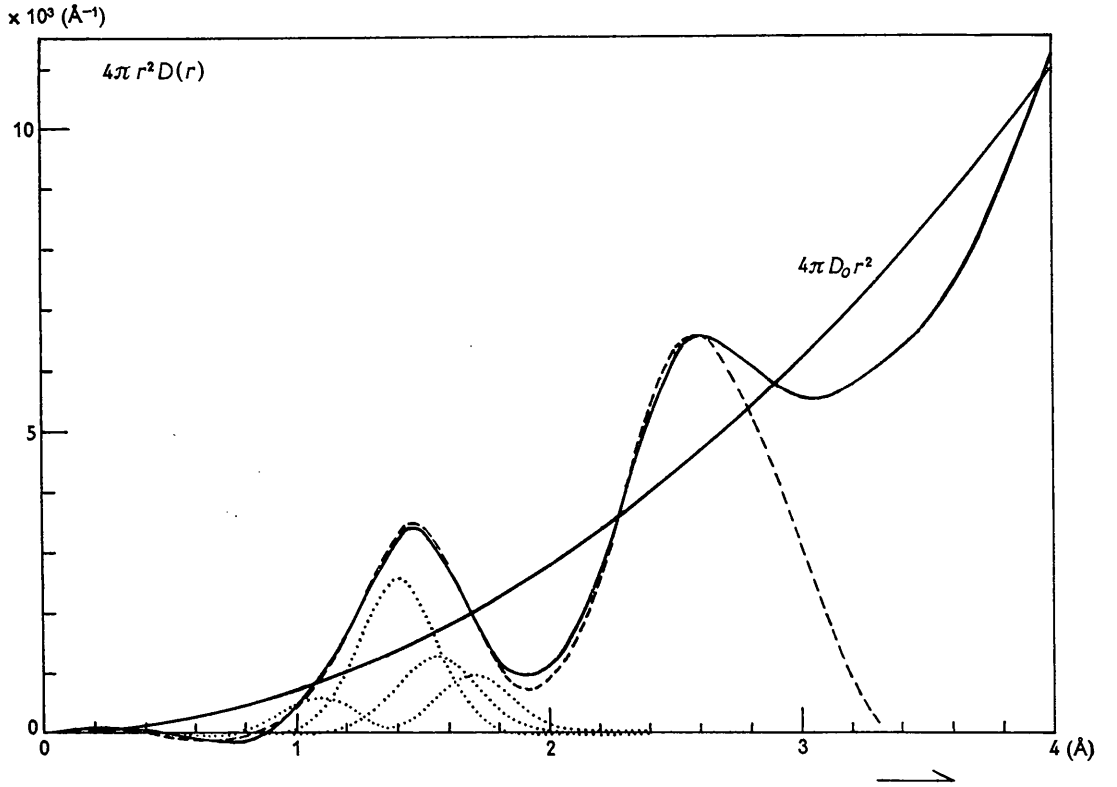

Fig. 8. Experimental curve of $4\pi r^2D(r)$ (full line) and curve calculated from equation (11) (broken line) for the Cl-derivative. Dotted curves show the individual peaks

where $A_{ij,k}$ and $a_{ij,k}$ are determined in order to satisfy the relation

$$\sum_{k=1} A_{ij,k} \exp(-a_{ij,k}s^2) = \exp(-as^2) \times \left[\frac{(Z_i - f_i(s))(Z_j - f_j(s)) \sum_{i}^{\text{unit}} (Z_i^2 + Z_i)}{Z_i Z_j \sum_{i}^{\text{unit}} \{(Z_i - f_i(s))^2 + s_i\}} - 1 \right]. \quad (12)$$

$4\pi r\Delta(r)$ was computed by the summation over integrands of equation (11) spaced at equal intervals of $\pi/20$ Å^{-1} with the value of $a = 0{\cdot}01$ Å^2. $4\pi r\Delta(r)$ and $4\pi r^2D(r)$ are shown in Figs. 7 and 8, respectively.

The curve of $4\pi r^2D(r)$ in the region of $r < 3$ Å was decomposed into individual peaks due to the interatomic distances by using the parameters listed in Table 4 and using the following values of $A_{ij,k}$ and $a_{ij,k}$:*

* In the present study, it was assumed, for simplicity, that the right side of equation (12) tends to zero as s approaches zero, namely, $\sum_{k=1} A_{ij,k} = 0$. Hence, equation (11) becomes

$$4\pi r\Delta(r) = \sum_{k=0}^{\infty} \sum_{i}^{\text{unit}} \sum_{j}' A_{ij,k}(Z_iZ_j/r_{ij}) \{4\pi(a_{ij,k} + \Delta_{ij})\}^{-\frac{1}{2}} \times \exp\{-(r - r_{ij})^2/4(a_{ij,k} + \Delta_{ij})\} - 4\pi r D_0^2$$

where $A_{ij,0} = 1$ and $a_{ij,0} = a$.

	$A_{ij,1}$	$a_{ij,1}$	$A_{ij,2}$	$a_{ij,2}$
C–C	0·20	0·025 Å^2	−0·20	0·60 Å^2
C–H	0·45	0·013	−0·45	0·35
C–Cl	−0·18	0·021	0·18	0·50
H–Cl	0·17	0·011	−0·17	0·20

In Fig. 8 the individual peaks are illustrated only for the first maximum of $4\pi r^2 D(r)$ along with the curve of the sum of all peaks listed in Table 4.

Table 4. *The values of parameters of the individual peaks in* $4\pi r^2 D(r)$ *for the* Cl-*derivative*

(C⋯C means the aromatic carbon–carbon bond.)

	r_{ij}	$(2\Delta_{ij})^{\frac{1}{2}}$	Scattering power
C⋯C	1·39 Å	0·05 Å	24 × 36 = 864
C—C	1·54	0·06	12 × 36 = 432
C—H	1·09	0·07	28 × 6 = 168
C—Cl	1·69	0·06	4 × 102 = 408
C⋯C⋯C	2·41	0·07	24 × 36 = 864
C—C—C	2·51	0·08	16 × 36 = 576
C⋯C—C	2·54	0·07	8 × 36 = 288
C⋯C—H	2·15	0·09	32 × 6 = 192
C—C—H	2·16	0·09	28 × 6 = 168
C⋯C—Cl	2·67	0·08	8 × 102 = 816
C ----- C	2·78	0·12	12 × 36 = 432
C ----- C	2·95	0·12	8 × 36 = 288
C ----- C	3·06	0·12	8 × 36 = 288
C ----- H	2·55	0·12	8 × 6 = 48
C ----- H	2·60	0·12	4 × 6 = 24
C ----- H	2·73	0·12	8 × 6 = 48
C ----- H	2·74	0·12	32 × 6 = 192
C ----- H	2·75	0·12	8 × 6 = 48
C ----- H	2·85	0·12	8 × 6 = 48
C ----- H	2·91	0·12	8 × 6 = 48
C ----- H	3·01	0·12	16 × 6 = 96
H ----- Cl	2·83	0·12	8 × 17 = 136

It was found from the radial distribution analysis that $4\pi r\Delta(r)$ had no appreciable fluctuation beyond $r = 4 \sim 6$ Å, and that the values of bond distances, bond angles, and mean deviations assumed in the calculation of intensities were reasonable.

6. Results and discussion

Intramolecular structure

The polymers used in this study were synthesized by a method of radical polymerization, and showed the halo patterns. Hence, these molecules have irregular structure, but there exist some orders within the nearest neighboring styrene residues, as shown by the analyses mentioned above.

Since the interatomic distances and especially the X–X distance of (iii), 5·04 Å, calculated from model I″ closely reproduced the intensity features of the observed patterns, and since a maximum appeared at 5 Å in the radial distribution curve, it is concluded that the structures of molecules of the *p*-halogen derivatives are that given by model I with ordinary values for bond distances and bond angles. The values of the C–X bond distances are found to be 1·69, 1·85 and 2·05 Å for Cl-, Br- and I-derivatives respectively, which are the values found in halogen derivatives of benzene. This arrangement of the residues is also found in syndiotactic polymers (Natta, 1955, 1956).

However, the remaining models or modifications such as a flexible chain structure or a spiral chain structure found in isotactic polymers have not yet been considered. In the case of polystyrene, Kakinoki (1949) concluded that, of the four models given in Fig. 2, models II and IV were unsatisfactory, but model III was not definitely ruled out. The substitution of heavy halogen atoms into polystyrene would be expected to give information in order to choose between models I and III. In the cases of *p*-derivatives, however, the intermolecular configuration must be considered together, for there are several intermolecular X–X distances smaller than the intramolecular X–X distances as given in Table 2(*b*). Some intensity curves were calculated for model III with a few intermolecular configurations, but they did not agree with the observed curves.

Intermolecular configuration

From comparison of the calculated intensities with the observed, model I_c was found to be better than models I_a and I_b for all halogen derivatives. The set of intermolecular X–X distances in model I_c, (i) the value equal to the van der Waals distance and (ii) 4·84, 4·85 or 4·93 Å for each derivative as shown in Table 2(*b*), are the most important parameters for giving the observed intensities. Since no other model having this set of X–X distances could be found, model I_c is the preferred structure in the films. It is very significant that the considerably different features of patterns for Cl-, Br- and I-derivatives can be explained with a single model of configuration.

Thus, it is concluded that the molecules of the *p*-halogen derivatives and, perhaps, of polystyrene with the intramolecular structure of model I″ are closely packed around each other as in model I_c, the 'face to face' arrangement in a plane perpendicular to the chain. Since this configuration was determined by using the set of X–X distances among the nearest neighbor molecules only, and since a large value of mean deviation, 0·23 Å, was found to be proper for these distances, the orientation of the next nearest and more distant molecules with respect to a given molecule must be nearly random.

A regularity in the configuration of the nearest neighbor residues was found even in the non-stereoregular polymers used in this study. It would be interesting to compare the present results with those obtained from a study of the same substances synthesized by stereospecific polymerization. The reason is that polymers of *p*-Cl- and *p*-Br-styrene have been reported to be amorphous even when they have been polymerized under the same conditions as used in obtaining crystalline polymers of styrene and *p*-F-styrene, but to turn into crystalline polymers by the complete catalytic hydrogenation of the

benzene rings accompanied by dehalogenation (Natta, 1960).

Method of analysis

The intensity formula of equation (4), on which the present analysis is based, represents the difference of the intensity diffracted by the actual distribution of atoms in a sample from that by a hypothetical, continuous medium having the average scattering power of the sample. A formula of this type, however, gives the observed intensity to a very good approximation except in the region of quite small s. Kakinoki (1949) and some other authors used an intensity formula of the type of

$$I(s) = (\text{summation term}) + \sum_{(AB)} k_{AB} \int_{l_{AB}}^{\infty} 4\pi r^2 \sin sr/sr\, dr \,. \quad (13)$$

This is formally the complete intensity, and is transformed into

$$I(s) = (\text{summation term}) - \sum_{(AB)} k_{AB} \int_{0}^{l_{AB}} 4\pi r^2 \sin sr/sr\, dr + \sum_{(AB)} k_{AB} \int_{0}^{\infty} 4\pi r^2 \sin sr/sr\, dr \,. \quad (14)$$

The first two terms are equal to equation (4), and the third represents the intensity from a continuous medium. Since Kakinoki omitted the third term in his calculation, his intensity curve inconsistently equals zero at $s=0$, while (13) has a positive, infinite value at $s=0$. In the present work, of course, the experimental intensity curves were extrapolated in order to tend to zero at $s=0$, as shown in Fig. 1. This difference is significant in the radial distribution analysis, since $4\pi r D(r)$ is obtained from the inversion of equation (13) and $4\pi r \Delta(r)$ from equation (3).

The method of calculation of the intensity described in Sec. 4 is useful for the study of the structure of a substance with large, relatively rigid groups of atoms as in the present case. In the procedure, however, it is troublesome to estimate the value of l_{AB}. It should be determined from the behavior of the radial distribution curve. Since it was found for the Cl-derivative that the fluctuation of the radial distribution function is small beyond $r=4$ to 6 Å, the values of l_{AB} assumed here are reasonable, and only a rough correction for the deviation of $W_{AB}(r)$ from unity beyond $r=l_{AB}$ is necessary. The values of l_{XX} assumed for Br- and I-derivatives are also reasonable, because the observed intensity features can be well reproduced using only the distances shorter than 6·0 Å. The method for the correction described in Sec. 4 is only a convenient one without use of the result of the radial distribution analysis. The residual scattering power, $\Delta\Psi$, was distributed to a few distances which belonged to the types of atomic pairs with large values of $\Delta\psi_{AB}$. The correction term could be more exactly calculated by considering the actual fluctuation of the radial distribution function in the region of $r > l_{AB}$.

In the method of comparison of intensities, the experimental intensity, equation (1), is converted into equation (4) assuming that both $(Z_i - f_i(s))/Z_i$ and $(S_i(s)/Z_i)^{\frac{1}{2}}$ have a similar angular dependence irrespective of the type of atom (equation (6)). This is satisfactory since the comparison was carried out mainly in the region of large s where the approximation was very good. On the other hand, the difference of these angular dependences, which is small but certainly exists, is taken into consideration in the radial distribution analysis by the method reported by Katada (1958). The usual way to diminish this effect (Bartell, Brockway & Schwendeman, 1955) is not adaptable to the case of non-gaseous substances because it is very difficult to calculate the intensity in the region of small s.

Outer halos

It is one of the characteristics in electron diffraction that many halos are observable over a wide range of s. Some authors (Coumoulos, 1943; Pinsker, 1953), however, have reported the appearance of only a small number of halos, usually not more than five, and attributed this to the nature of the aggregation of atoms in an amorphous state. This may be incorrect, and the reason for a small number of observable halos could be attributed to the fact that the films used were so thick that outer halos were masked by the intense background. The aggregation of atoms in amorphous substances is essentially similar to that in gases or in liquids from the standpoint of diffraction phenomena.

Many outer halos, in fact, have been obtained by the author in a reexamination of thin films of methyl methacrylate which was reported to give only four maxima by Coumoulos (1943). The electron diffraction pattern showed halos at $s=12{\cdot}81$, $16{\cdot}21$, $17{\cdot}87$, $20{\cdot}96$ and $24{\cdot}60$ Å^{-1} and a few rings as well as halos in the region of $s<10$ Å^{-1}, some of which corresponded to those obtained by Coumoulos.

The author wishes to express his thanks to Prof. J. Kakinoki for his continuing interest and encouragement during the course of this investigation. He is also grateful to Dr T. Ino for valuable discussion. The author also expresses his thanks to the Osaka Municipal Office for making available to him a set of electrical accounting machines of I.B.M. Corporation.

References

Bartell, L. S., Brockway, L. O. & Schwendeman, R. H. (1955). *J. Chem. Phys.* **23**, 1854.

Coumoulos, G. D. (1943). *Proc. Roy. Soc. London*, A, **182**, 166.

GLAUBER, R. & SCHOMAKER, V. (1953). *Phys. Rev.* **89**, 667.
IBERS, J. A. & HOERNI, J. A. (1954). *Acta Cryst.* **7**, 405.
INO, T. (1953). *J. Phys. Soc. Japan*, **8**, 92.
KAKINOKI, J. (1949). Scientific Papers from the Osaka University. No. 16.
KAKINOKI, J., MURATA, H. & KATADA, K. (1949). Scientific Papers from the Osaka University. No. 17.
KARLE, I. L. & KARLE, J. (1949). *J. Chem. Phys.* **17**, 1052.
KARLE, J. & KARLE, I. L. (1950). *J. Chem. Phys.* **18**, 957.
KATADA, K. (1958). *J. Phys. Soc. Japan*, **13**, 51.
NATTA, G. (1955). *Makromol. Chem.* **16**, 213.
NATTA, G. (1956). *Angew. Chem.* **68**, 395.
NATTA, G. (1960). *Makromol. Chem.* **35**, 94.
PAULING, L. (1960). *The Nature of the Chemical Bond.* Ithaca: Cornell University Press.
PAULING, L. & BROCKWAY, L. O. (1934). *J. Chem. Phys.* **2**, 867.
PINSKER, Z. G. (1953). *Electron Diffraction.* (Translated by SPINK, J. A. & FEIGL, E.) London: Butterworths Scientific Publications.
SUTTON, L. E. (1958). *Tables of Interatomic Distances and Configuration in Molecules and Ions.* London: The Chemical Society.

Acta Cryst. (1963). **16**, 301

La Structure des Colloides d'Association. VIII. Description de la Structure des Savons de Cadmium à Température Elevée

PAR P. A. SPEGT ET A. E. SKOULIOS

Centre de Recherches sur les Macromolécules, 6, rue Boussingault, Strasbourg, France

(*Reçu* 19 *juillet* 1962)

An X-ray diffraction study of pure cadmium soaps has been carried out between 50 and 250 °C. The structure of the mesomorphic phase occurring between 100 and 200 °C. has been described as corresponding to the packing of cylindrical structural elements according to a two-dimensional hexagonal array. Parameters, such as number of polar groups per unit length and radii of the polar regions within the structural elements, have been determined.

Introduction

On a récemment décrit la structure des phases mésomorphes que présentent les savons de sodium purs à température élevée (Skoulios & Luzzati, 1961). En examinant le mode d'assemblage des extrémités polaires des molécules de savon dans ces phases on a pu les classer en deux groupes bien distincts: Le premier groupe est caractérisé par la localisation des extrémités polaires dans des rubans de largeur petite et de longueur indéfinie; l'édifice ainsi constitué est compact, analogue à celui existant dans les cristaux. Dans le deuxième groupe les parties polaires sont localisées en double couche dans des feuillets indéfinis; leur assemblage y est désordonné et labile comme dans un liquide à deux dimensions.

A la lumière de ces résultats, il était important d'examiner en détail le rôle du cation dans l'édification de ces structures. Deux voies complémentaires pouvaient être tracées: l'étude des sels d'acides gras des métaux du groupe du sodium (lithium, potassium, *etc.* ...) et celle des savons d'autres métaux, divalents ou trivalents. Alors que la première étude est poursuivie actuellement par ailleurs (Gallot & Skoulios, 1962), nous avons entrepris celle des savons de métaux alcalinoterreux (Spegt & Skoulios, 1960, 1962). Dans ce mémoire nous décrivons les résultats obtenus pour les savons de cadmium anhydres, qui par la simplicité de la structure de leurs phases mésomorphes à température élevée, en permettent une étude détaillée.

Parmi les nombreuses études dont les savons métalliques ont été l'objet, même la plus complète, celle de Vold *et al.* (Vold & Hattiangdi, 1949; Hattiangdi & Vold, 1949), n'apporte pas de renseignements sur la structure des phases mésormorphes rencontrées à température élevée. Cela est dû à l'insuffisance de la technique expérimentale de diffraction des rayons X employée par ces auteurs.

Techniques experimentales

Les savons* que nous avons utilisés ont été préparés de la manière décrite par Vold & Hattiangdi (1949) par action directe du chlorure de cadmium sur le savon de sodium correspondant, en solution alcoolique. La purification des savons obtenus a été opérée de façon différente; nous avons d'abord lavé le produit à l'eau bouillante, puis à l'éther et enfin nous l'avons séché à 90 °C. sous vide. Nous avons contrôlé que les

* La formule chimique générale des savons de cadmium est:

$$[CH_3\text{-}(CH_2)_{n-2}\text{-}COO]_2Cd$$

$n=12$	laurate de cadmium	($C_{12}Cd$)
$n=14$	myristate de cadmium	($C_{14}Cd$)
$n=16$	palmitate de cadmium	($C_{16}Cd$)
$n=18$	stéarate de cadmium	($C_{18}Cd$)
$n=20$	arachidate de cadmium	($C_{20}Cd$)